PNAS
www.pnas.org

Supplementary Information for
Lipid droplets in mammalian eggs are utilized during embryonic diapause.

Roberta Arena[#], Simona Bisogno[#], Łukasz Gąsior[#], Joanna Rudnicka, Laura Bernhardt, Thomas Haaf, Federica Zacchini, Michał Bochenek, Kinga Fic, Ewelina Bik, Małgorzata Barańska, Anna Bodzoń-Kułakowska, Piotr Suder, Joanna Depciuch, Artur Gurgul, Zbigniew Polański, Grażyna E. Ptak.

Grażyna E. Ptak
Email: g.ptak@uj.edu.pl

This PDF file includes:

Supplementary text
Figures S1 to S2
Legends for Movies S1 to S11
SI References

Other supplementary materials for this manuscript include the following:

Movies S1 to S11

Supplementary information text

Supplementary Methods

Matrix-assisted laser desorption ionization – time of flight mass spectrometry (MALDI-TOF MS). Data imaging and analysis were performed using an UltrafleXtreme MALDI-TOF/TOF instrument (Bruker Daltonics, Bremen, Germany). The TOF analyser was set in the reflectron mode. At the time of analysis, the embryos were thawed and fixed in 4% paraformaldehyde for 20 min and washed first in 0.4% PBS-PVP and then in ultrapure water. Samples were placed on indium tin oxide (ITO) glass slides and allowed to dry at room temperature under vacuum. Phosphatidylcholine and phosphatidylinositol were measured in positive and negative ion modes, respectively. For the positive ion mode, 2,5-dihydroxybenzoic acid (DHB) matrix was prepared in a concentration of 30 mg/ml in methanol/water solution (1:1, v/v), then trifluoroacetic acid was added (0.2% v/v), according to the mass spectrometer manufacturer's recommendation. For the negative ion mode, 9-aminoacridine (9AA) matrix was prepared in a concentration of 10 mg/ml in ethanol/water solution (70:30, v/v). The matrices were deposited on the samples using an ImagePrep device (Bruker Daltonics, Bremen, Germany) based on a standard ImagePrep protocol for DHB and a protocol for alpha-cyano-4-hydroxycinnamic acid for 9AA deposition. Mass spectra were acquired as follows: the scan range was 300–3000 m/z, the laser power was set to 20%, and matrix suppression was turned off. Holder's random walk was limited to 200 µm diameter in "partial sample" mode, with 500 shots at a raster spot. In a single cycle, sum of 5000 laser shots were used for spectrum acquisition. Two cycles (10,000 laser shots) were used to acquire the final spectrum. For lipid identification, fragmentation based on the LIFT technology was used. The parent ion was manually selected for every acquired MS/MS spectrum.

Fourier Transform Raman spectroscopy (FT-Raman). FT-Raman spectra were recorded using a Nicolet NXR 9650 FT-Raman spectrometer (Thermo Fisher Scientific) equipped with an Nd:YAG laser (1064 nm) and a germanium detector. Measurements of were performed in the range from 150 to 3700 cm−1 with a laser power of 1 W. Unfocused laser beam was used with a diameter of approximately 100 µm and a spectral resolution of 8 cm−1. Raman spectra were processed by the Omnic/Thermo Scientific software based on 64 scans. In the obtained spectra, baseline correction and normalization was performed prior identifying the bands belonging to chemical compounds. Then, arithmetic mean wavenumber values were assigned to particular functional groups to calculate the ratio of the intensity values of lipids for individual groups. To obtain information about the spectra variation, the PCA analysis was performed. In order to indicate the groups of the individual species with the highest similarity in respect to the absorbance spectra, hierarchical clustering analysis (HCA) with Euclidean distance and Ward's algorithms was used. This method was applied for the ranges between 800 – 1800 cm-1 ("fingerprint region"). Statistical and multidimensional analysis was done using PAST software[1-8].

Embryo immunofluorescence staining. After fixation, blastocysts were washed in PBS and permeabilized with 0.5% Triton X-100 in PBS for 20 min at room temperature. Then, blastocysts were quenched with 2.5 mg/ml NH4Cl in PBS for 10 min and blocked with 10% fetal bovine serum and 0.005% Tween-20 in PBS (block solution) for 1 h at room temperature. Blastocysts were incubated overnight at 4°C with one the following primary antibodies in block solution: anti-ECI1 antibody (Biorbyt, 1:300), anti-ACOX1 (Bioss Antibodies, 1:300), anti-ACOX2 antibody (Proteintech Group, 1:100), anti-ACOX3 antibody (Bio-Techne, 1:50), and anti-ACSL1 antibody (Bio-Techne, 1:100). After washing with block solution, the blastocysts were incubated for 1 h at room temperature with the secondary conjugated antibody Cy™3 AffiniPure Donkey Anti-Rabbit

(Jackson ImmunoResearch, 1:600) in block solution. Then, samples were rinsed three times, with each rinsing lasting 10 min, in 0.4% PBS-PVP and were labeled with high-content screening (HCS) CellMask™ Blue cytoplasmic/nuclear stain (Invitrogen), according to the manufacturer's instructions. Mounted specimens were analysed with a confocal ZEISS LSM 880 Confocal Laser Scanning Microscope using 20x Zeiss Plan-Apochromat Infinitive corrected objective with a numerical aperture of 0.8.

Supplementary figures

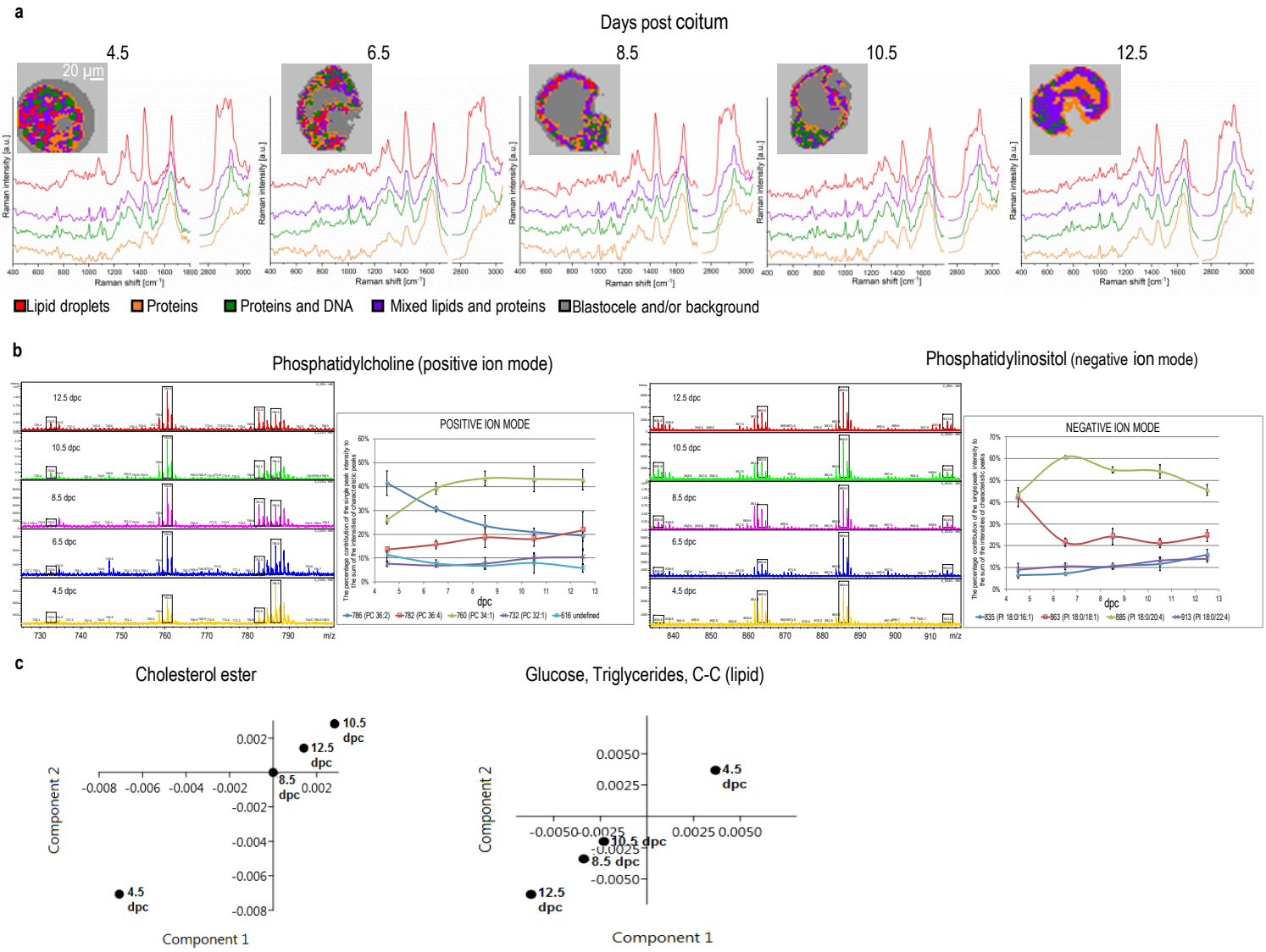

Fig. S1. **a)** Confocal Raman imaging data processing. Representative K–Means Clustering (KMC) analysis for a blastocyst at each dpc analysed. The spectra grouping into 5 classes each of them coded by a color as indicated in the legend. **b)** Phosphatidylcholine (PC) and phosphatidylinositol (PI) fingerprint in diapausing blastocysts detected by MALDI TOF/TOF MS. The right side of the panel show the fragment spectra of the of diapausing blastocyst for positive ion mode. The squares indicate peaks of PCs, the intensity of a single peak was referred to the sum of all the characteristic peaks and presented as a percentage for the particular dpc. The left side of the panel show the fragment spectra of the of diapausing blastocyst for negative ion mode. The squares indicate peaks of PIs, the intensity of a single peak was referred to the sum of all the characteristic peaks and presented as a percentage for the particular dpc. **c)** PCA analysis of embryo collection media at 4.5 dpc; 8.5 dpc; 10.5 dpc; 12.5 dpc. Left Two-dimensional (2D) scores plot of embryo collection media indicates differences in the spectral regions of cholesterol ester at 10.5 and 12.5 vs 4.5 dpc by FT-Raman. Right Two-dimensional (2D) scores plot of embryo collection media shows differences in the spectral regions of glucose, triglycerides and C-C lipid at 8.5, 10.5 and 12.5 vs 4.5 dpc by FT-Raman.

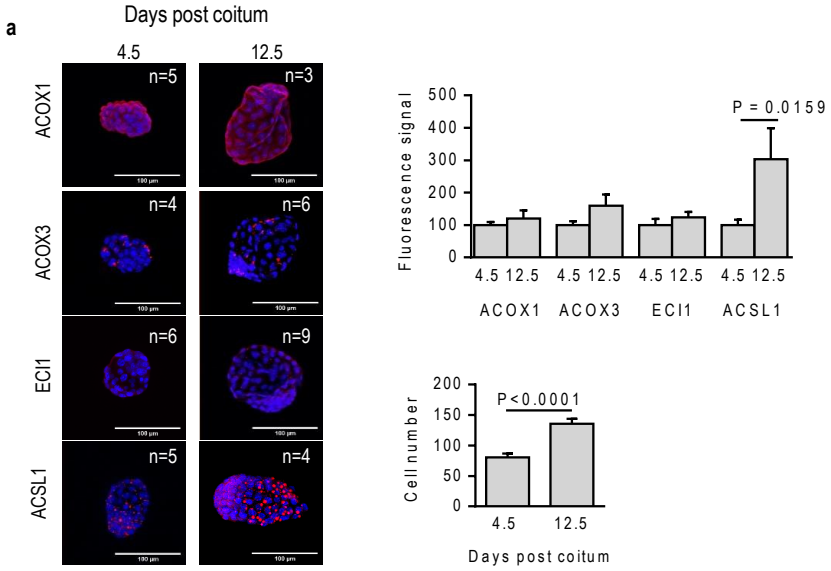

Fig. S2. a) Diapausing blastocyst immunolabeled for Acox1, Acox3, Eci1, and Acsl1, and DAPI staining at 4.5 and 12.5 dpc. n=number of blastocysts. Scale bar=100 µm. The top-right histogram shows higher fluorescence for Acsl1 in blastocysts at 12.5 vs. 4.5 dpc. The bottom-right histogram indicates increased cell numbers in blastocysts at 12.5 dpc vs. 4.5. n≥ 10. Values are mean ± SEM; two-tailed unpaired Student's t-test.

Movie S1. Micromanipulation procedure of delipidation of the zygote.

Movie S2. CARS. LDs visualization in mammalian oocytes: rat.

Movie S3. CARS. LDs visualization in mammalian oocytes: European hedgehog.

Movie S4. CARS. LDs visualization in mammalian oocytes: mouse.

Movie S5. CARS. LDs visualization in mammalian oocytes: long-tailed chinchilla.

Movie S6. CARS. LDs visualization in mammalian oocytes: bank vole.

Movie S7. CARS. LDs visualization in mammalian oocytes: guinea pig.

Movie S8. CARS. LDs visualization in mammalian oocytes: short-tailed weasel.

Movie S9. CARS. LDs visualization in mammalian oocytes: roe deer.

Movie S10. CARS. LDs visualization in mammalian oocytes: American mink.

Movie S11. CARS. LDs visualization in mammalian oocytes: European badger.

SI References

References:

1. Gualerzi, A. et al. Raman spectroscopy uncovers biochemical tissue-related features of extracellular vesicles from mesenchymal stromal cells. Sci. Rep. 7, (2017).
2. Chan, J. W. et al. Micro-raman spectroscopy detects individual neoplastic and normal hematopoietic cells. Biophys. J. 90, 648–656 (2006).
3. Krafft, C., Neudert, L., Simat, T. & Salzer, R. Near infrared Raman spectra of human brain lipids. Spectrochim. Acta - Part A Mol. Biomol. Spectrosc. 61, 1529–1535 (2005).
4. Silveira, L. et al. Correlation between near-infrared Raman spectroscopy and the histopathological analysis of atherosclerosis in human coronary arteries. Lasers Surg. Med. 30, 290–297 (2002).
5. Stone, N., Kendall, C., Smith, J., Crow, P. & Barr, H. Raman spectroscopy for identification of epithelial cancers. Faraday Discuss. 126, 141–157 (2004).
6. Huang, Z. et al. Near-infrared Raman spectroscopy for optical diagnosis of lung cancer. Int. J. Cancer 107, 1047–1052 (2003).
7. Huang, Z. et al. Effect of formalin fixation on the near-infrared Raman spectroscopy of normal and cancerous human bronchial tissues. Int. J. Oncol. (2003).
8. Stremersch, S. et al. Identification of Individual Exosome-Like Vesicles by Surface Enhanced Raman Spectroscopy. Small 12, 3292–3301 (2016).